JOINT EUROPEAN TORUS JET

JET–P(93)94

J.P. Goedbloed, H.A. Holties, S. Poedts, G.T.A Huysmans, W. Kerner

MHD Spectroscopy: Free Boundary Modes (ELMs) & External Excitation of TAE Modes

MHD Spectroscopy: Free Boundary Modes (ELMs) & External Excitation of TAE Modes

J.P. Goedbloed[1], H.A. Holties[1], S. Poedts[1], G.T.A Huysmans, W. Kerner

JET-Joint Undertaking, Culham Science Centre, OX14 3DB, Abingdon, UK

[1]FOM-Instituut voor Plasmafysica, Nieuwegein, The Netherlands.

Preprint of a paper to be submitted for publication in
Plasma Physics and Controlled Fusion
October 1993

ABSTRACT

Limitations of present knowledge of plasma equilibrium profiles hamper a proper identification of MHD modes. However, through continued improvement of both numerical calculations and experimental observations we may witness the birth of a new kind of spectroscopy, properly called MHD spectroscopy, in the coming decade. This is illustrated by studies of Edge Localised Modes and external excitation of Toroidal Alfvén Eigenmodes.

1. INTRODUCTION

1.1 Context

Recent studies of Edge Localised Modes (ELMs) in JET and the prospect of external excitation, and even control, of Toroidal Alfvén Eigenmodes (TAEs) point to the importance of free boundary magnetohydrodynamic (MHD) modes. This involves a coupling of the plasma to the outside 'world' through the motion of the plasma boundary, which is caused internally by ELMs or externally by the excitation through an antenna system. The two kinds of dynamics correspond to two different theoretical points of view (see section 2.2), viz. calculation of the spectrum of relevant free boundary modes (passive perturbation of the boundary) or computation of the plasma response to an external driving force (active perturbation of the boundary). Both points of view are just the different representations of MHD spectral theory, which is of central importance for the understanding of plasma dynamics on the Alfvén time scale. In previous papers [1, 2] the term MHD spectroscopy has been introduced in this context to indicate that this field holds promises for the understanding of magnetically confined plasma structures, similar to the understanding of atomic phenomena brought about by the advent of atomic spectroscopy and quantum mechanics.

Crucial for progress in this field is the improvement of numerical calculation and experimental identification of the modes and the continual interplay between these two activities. An example of what may be achieved is offered by the study of solar oscillation (section 1.2). Section 2 is devoted to the general theoretical framework of ideal and resistive MHD spectral calculations (the CASTOR code). This is applied in section 3 to the study of the influence of edge equilibrium profiles, resistivity, and plasma cross section of ELMs in JET and in section 4 to the study of external excitation of TAE modes by means of the

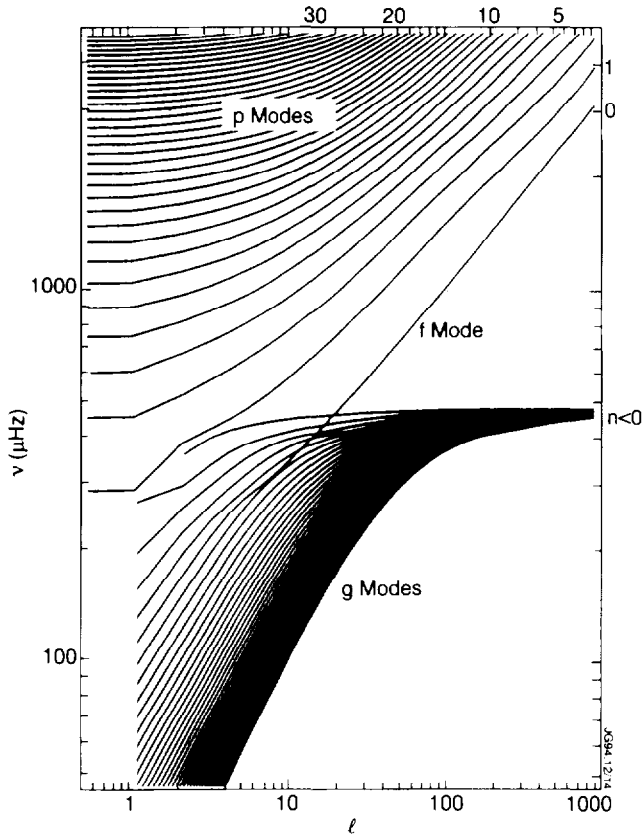

Fig.1. Solar Oscillations for Standard Solar Model (Courtesy of J. Christensen-Dalsgaard).

planned experiment at JET exploiting the saddle coils for disruption control. Conclusions are drawn in section 5.

1.2 Example: Helioseismology

The study of the global oscillations of the sun offers the pertinent angle relevant for our study. The essential point of view is that of gas dynamics, which considers the sun as a spherical gas, internally heated by thermonuclear reactions in the core, and held together by gravity. This leads to the standard solar model concerned with the construction of a consistent picture of the gas dynamic aspects of the sun. One of the triumphs of this view point is the development of a new field of research called helioseismology (see, e.g. chapter VII of Ref. 3). This is best illustrated by means of the spectrum of solar oscillations calculated for a standard solar model (Fig. 1, obtained from Ref. 4). Here, the two branches of the spectrum, viz. the acoustic (p and f) and the gravity (g) modes, are shown as calculated from a spherically symmetric model. It turns out that the frequencies deduced from the Doppler shifts of spectral lines agree with the calculated ones for the p-modes to

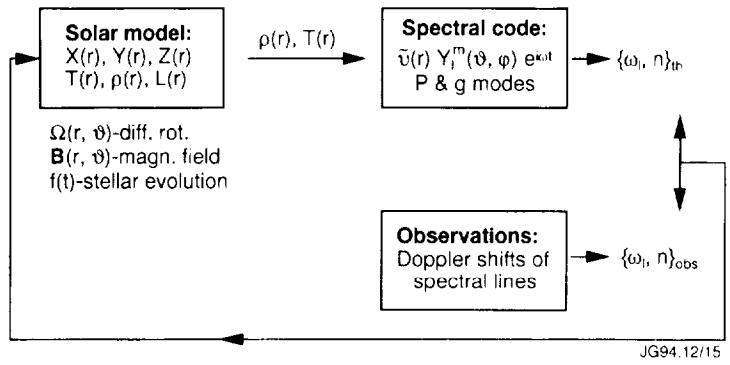

Fig.2. Systematics of Helioseismology.

within 0.1%! This impressive agreement serves as an example for what is possible in a purely classical, fluid dynamical kind of spectroscopy.

Notice that for the birth of helioseismology it was not sufficient to have collected a great number of observations of solar oscillations or to have calculated many spectra, but rather that the two activities should have matured to a sufficient degree so as to allow for a unique correlation between calculated and observed spectra. This interplay between theory and observations is illustrated in Fig. 2. To leading order the Solar Model is spherically symmetric with the equilibrium depending on the abundance of the different chemical elements H, He, etc. (indicated by X, Y, Z), the temperature T, the density ρ, the luminosity L, etc. Perturbations of this equilibrium are studied by means of a Spectral Code which determines the different frequencies $\omega_{l,\,n}$ of the different modes. Observations provide information on the same quantities. The discrepancies between the two then being about improved assumptions on the Solar model, where the non-spherical symmetry due to the presence of differential rotation (Ω) and magnetic fields **(B)** plays and important role. Of Course, the final interest is in stellar evolution, i.e. the very slow time-dependence of all the equilibrium quantities. It is not difficult to recognise the counterparts of the three activities depicted in Fig. 2 for fusion research: slow transport, fast MHD modes, and diagnostics to determine the character of these modes. Clearly, the success of this scheme hinges on improved diagnostics and spectral calculations. Helioseismology provides the paradigm demonstrating that fluid dynamical states can be predicted with high accuracy.

2. SPECTRAL MHD CALCULATIONS

2.1 General Framework

Our starting point is the set of resistive MHD equations which govern the temporal evolution of the density ρ, the velocity $\mathbf{v}$, the temperature T, and the magnetic field $\mathbf{B}$:

$$\frac{\partial \rho}{\partial t} = -\nabla \cdot (\rho \mathbf{v}), \tag{1}$$

$$\rho \frac{d\mathbf{v}}{dt} = -\nabla p + \frac{1}{\mu_0}(\nabla \times \mathbf{B}) \times \mathbf{B} + \rho \mathbf{g}, \tag{2}$$

$$C_v \rho \frac{dT}{dt} = -p \nabla \cdot \mathbf{v} + \frac{\eta}{\mu_0^2}(\nabla \times \mathbf{B})^2, \; p = (\gamma - 1) C_v \rho T, \tag{3}$$

$$\frac{\partial \mathbf{B}}{\partial t} = \nabla \times (\mathbf{v} \times \mathbf{B}) - \frac{1}{\mu_0} \nabla \times (\eta \nabla \times \mathbf{B}), \; \nabla \cdot \mathbf{B} = 0. \tag{4}$$

The gravity term in Eq. (2), which is just included as a reminder of its importance in astrophysics, will not play any further role in the present discussion. In ideal MHD (η = 0), it is convenient to exploit the pressure p as a variable rather than T. In that case the four equations just express conservation of mass, momentum, entropy, and magnetic flux.

Let us now linearise the equations (1) - (4). For definiteness, consider a static 2D equilibrium and linearise according to

$$f(\mathbf{r}, t) \approx f_0(\Psi, \theta) + f_1(\Psi, \theta) e^{i(n\phi - \omega t)}, \tag{5}$$

where Ψ, θ, and ϕ refer to some toroidal co-ordinate system for tokamaks with ignorable co-ordinate ϕ, and n is the toroidal mode number.
For ideal MHD, writing $\mathbf{v}_1 \equiv \partial \xi / \partial t$, three of the four conservation equations can be integrated directly and we are led to the spectral problem

$$\mathbf{F}(\xi) = -\rho \omega^2 \xi, \tag{6}$$

where **F** is the well-known force operator [5], which is self-adjoint, and the eigenvalue ω^2 is real.

For resistive MHD this scheme does not work and we are forced to consider the eight components describing the perturbed state. Exploiting a description in terms of the perturbed vector potential **A** entering the basic state vector.

$$\mathbf{U} \equiv [\rho_1,\ \mathbf{v},\ T_1,\ \mathbf{A}]^T \tag{7}$$

(an 8-vector), the linearised system of equations is written in the matrix form

$$\mathbf{L} \cdot \mathbf{U} = \lambda \mathbf{R} \cdot \mathbf{U}. \tag{8}$$

Eq. (8) is solved by the Galerkin method: A weak form is constructed by multiplying with arbitary test functions **V** and integrating over the domain of interest, i.e. the plasma interior:

$$\int \mathbf{V}^T \cdot \mathbf{L} \cdot \mathbf{U}\ dV = \lambda \int \mathbf{V}^T \cdot \mathbf{R} \cdot \mathbf{U}\ dV. \tag{9}$$

U is a solution of Eq. (8) in the weak sense if Eq. (9) is satisfied for every test function **V** of the appropriate space, satisfying the boundary conditions.

Discretisation (by means of finite elements for the Ψ-dependence and fast Fourier transforms for the θ-dependence) results in the non-symmetric spectral problem

$$\mathbf{A} \cdot \mathbf{x} = \lambda \mathbf{B} \cdot \mathbf{x}, \tag{10}$$

where **A** and **B** are large non-Hermitian matrices [6] and $\lambda \equiv -i\omega$ is the complex eigenvalue. Apart from the necessary construction of the equilibrium (by means of the HELENA code [7]), this is the core of the problem solved by the CASTOR code.

2.2 Extension to Free Boundary Modes

To study free-boundary modes, CASTOR has been extended with an external vacuum magnetic field perturbation in two ways:

- *Passive perturbation of the boundary* (e.g. by ELMs: see section 3). The vacuum magnetic field perturbation $\hat{\mathbf{b}} = \nabla\hat{\mathbf{\Phi}}$ satifies Laplace's equation

$$\nabla^2\hat{\mathbf{\Phi}} = 0. \tag{11}$$

This equation is solved again by the Galerkin method with a given plasma boundary perturbation. The response of the tangential field to the normal field perturbation is extracted from this solution:

$$\hat{\phi}_m = \sum_{m'} \alpha_{mm'} \left(\hat{j}\hat{b}^1\right)_{m'}. \tag{12}$$

This may be considered to be the discretised form of Green's theorem. The matrix $\alpha_{mm'}$ enters boundary integrals resulting again in the eigenvalue problem (10), with modified matrices **A** and **B** [8].

- *Active perturbation of the boundary* (e.g. by an external antenna exciting TAE modes: see section 4). Here, the response changes to:

$$\hat{\phi}_m = \sum_{m'} \alpha_{mm'} \left(\hat{j}\hat{b}^1\right)_{m'} + \beta_m^{ant}, \tag{13}$$

where β^{ant} is the driven vacuum solution with unperturbed boundary. This results in a forced oscillation problem involving the same matrices **A** and **B**:

$$\left(\mathbf{A} + i\omega_d \mathbf{B}\right)\cdot\mathbf{x} = \mathbf{f}, \tag{14}$$

where ω_d is the driving frequency and **f** is the driving term involving the quantities β_m^{ant}. For numerical purposes the driven problem (14) is simpler than the corresponding spectral problem (10) since it does not require the computation of the full spectrum.

3. FREE BOUNDARY RESISTIVE MODES AND ELMS

3.1 H-Mode and ELMs in Tokamaks

Recall the context in which ELMs occur, viz. the H-mode confinement regime in tokamaks [9] characterised by:

- Improved confinement due to the suppression of the plasma edge turbulence. For future fusion reactors, the obvious benefit arising from an increase of the thermal pressure by a factor of 2 is the increase of the thermonuclear power output by a factor of 4.

- Large edge gradients ∇T and ∇n (and also large gradients in the shear flow and associated radial electric field according to [9], but see also [10]).

- The H-mode may be terminated by repetitive MHD events. In particular, ELMs may destroy the required transport barrier.

- On the other hand, ELMs may control the impurity content so that the quasi-stationary state H-mode operation is facilitated (with somewhat reduced confinement through).

From previous MHD studies of ELMs in JET [11] it has become clear that crucial elements are a local steepening of the edge pressure and current density profiles during the H-mode phase. Moreover, ELMs occur at values of β far below the ideal ballooning limit. Since ELMs may be triggered by a decrease of the edge temperature by gas puffing, on the one hand, and may be stabilised by heating of the edge, on the other hand, it is concluded that ELMs are resistive rather than ideal MHD modes. This could include both resistive ballooning modes (large n), driven by the p' profile, and low-n free-boundary resistive modes with a large radial extent, driven by the $j\phi$ and $j'\phi$ profiles. However, since ELMs cause a large perturbation of the plasma boundary with concomitant expulsion of particles and energy, it is proposed that the latter modes are the relevant instabilities.

3.2 ELMs in JET

As a first example of MHD spectroscopy let us then consider the study of ELMs in JET by means of CASTOR. Departing from experimental data, which to date are not sufficiently precise to either prove or exclude a certain instability, we will just consider the different low-n free-boundary modes compatible with the given data. Thus, the basic activity consists of playing with the equilibrium profiles to narrow down the number of possibilities. We consider three cases:

- *Influence of the edge current density* j_ϕ (JET #23336). In Fig. 3 both the electron pressure profile as measured by LIDAR (dotted line) and the

reconstructed equilibrium profiles are shown. Clearly, reasonable agreement has been obtained, but not to a sufficient degree to prove or disprove the presence of large current gradients to drive external resistive instabilities. This is demonstrated by Fig. 4 which shows the growth rate of the n = 1 free-boundary tearing mode for three choices of the current density profile. Whereas the reconstructed profile (labelled by 1) produces a growth rate that is insignificant for the relevant values of the edge resistivity, and artificial increase of the shoulder on the current density profile (curve labelled by 3) produces growth rates that are both significant and show the required threshold which would facilitate the occurrence of ELMs by a sudden increase of the resistivity due to edge cooling.

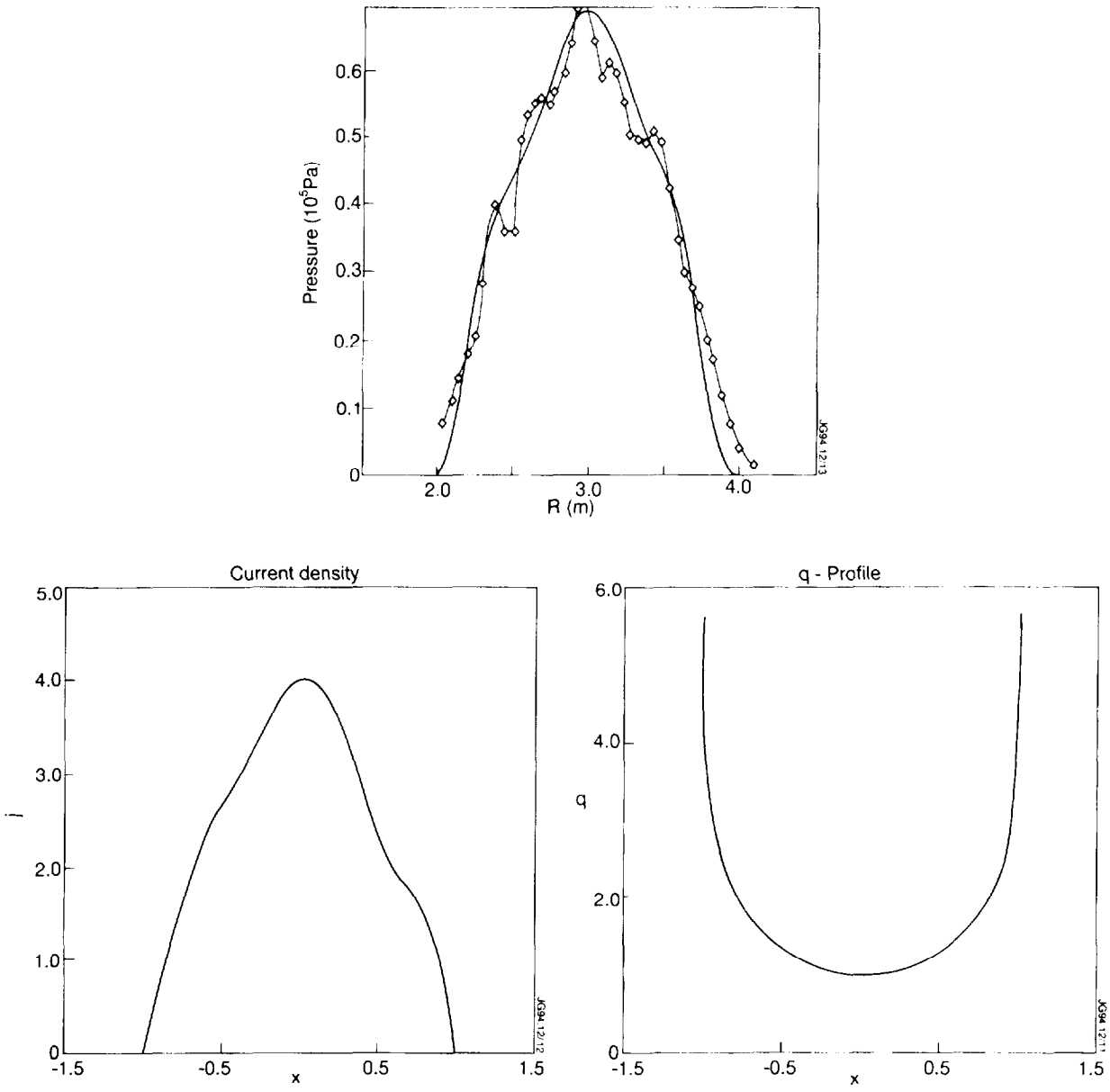

Fig.3. Reconstruction of Equilibrium Profiles (JET#23336)

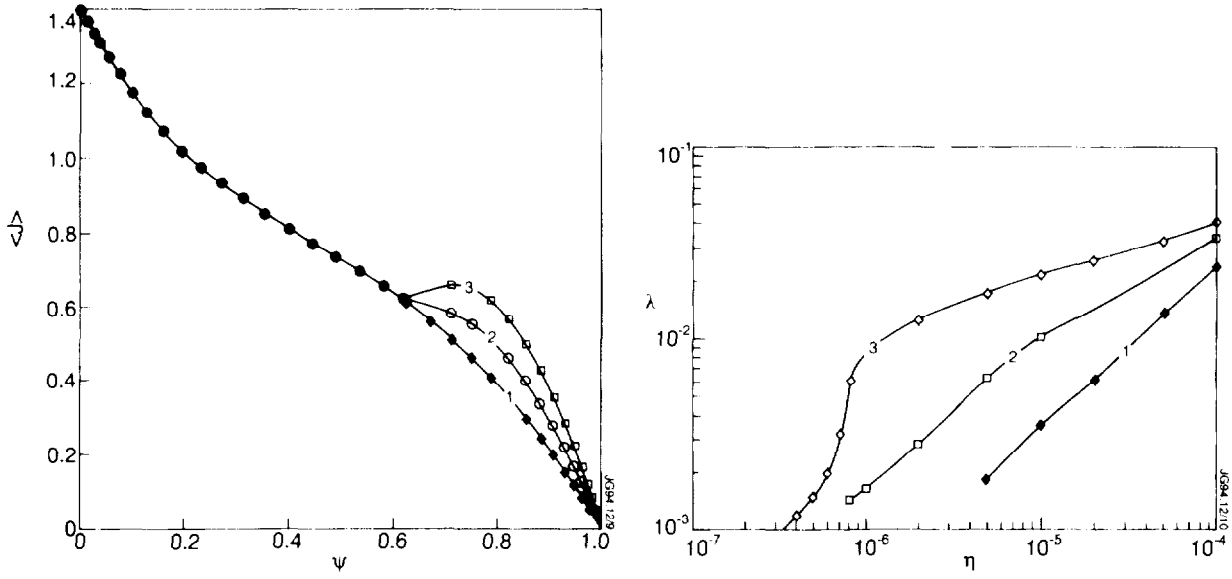

Fig.4. Flux Surface Averaged Toroidal Current Profiles and Corresponding Growth Rates as a Function of the Resistivity for the n = 1 Free Boundary Tearing Modes.

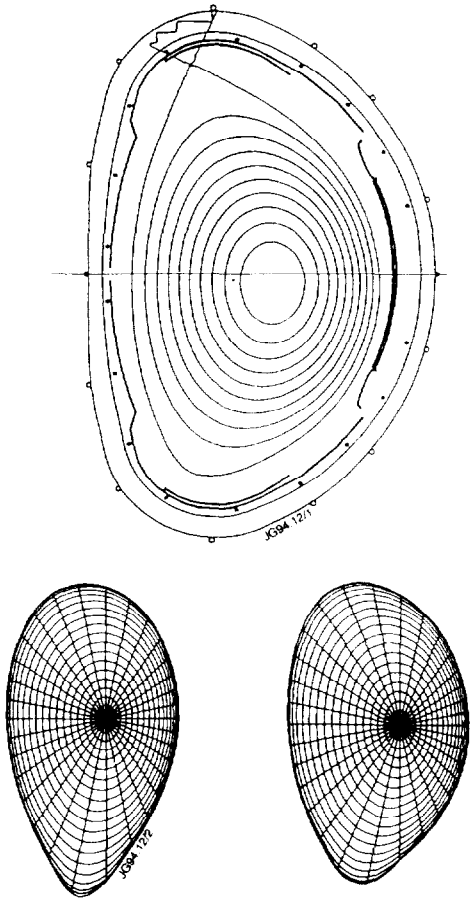

Fig.5. Plasma Shape of JET Discharges #26087 (above) and New Divertor Plasma Cross Sections ('Slim' and 'Fat' Configuration).

- *Influence of the pressure profile and the plasma cross section* (JET high performance shot #26087 and future divertor geometry). As an intermezzo, we consider the problem of ideal stability of JET discharges with respect to the dependence on the cross section, taking the discharge with the highest performance in the preliminary tritium campaign as a reference case. The procedure is to depart from the measured equilibrium profiles and corresponding plasma cross section of shot #26087, then to increase the local pressure gradient up to the ideal ballooning ($n = \infty$) limit everywhere, next to increase the total pressure until the ideal $n = 1$ external kink stability limit is reached, and finally to change the plasma cross section to correspond to the future pumped divertor geometry. The geometries are shown in Fig. 5. The 'slim' plasma shape is characterised by a larger connection length and will be used for divertor studies, whereas the 'fat' plasma shape has a larger volume and will be used in performance optimisation studies.

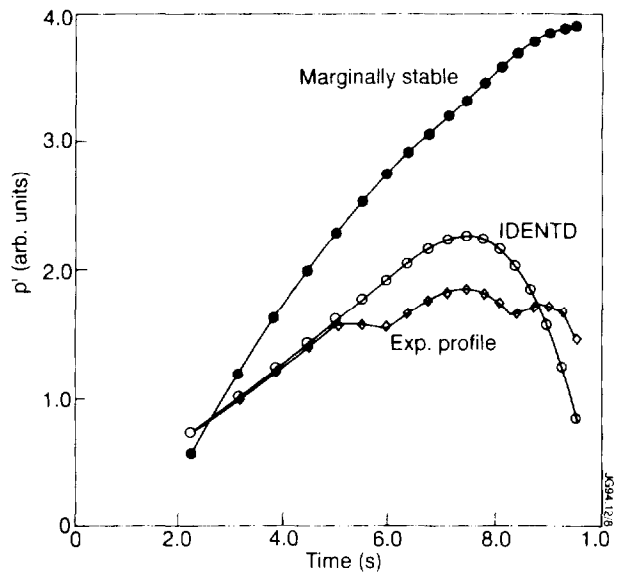

Fig.6. Experimental profiles of the Pressure Gradient Obtained from LIDAR and as Reconstructed by IDENTD (JET #23336) and Constructed Marginally Stable Pressure Gradient profile with the Corresponding Values of β for the Three Plasma Cross Sections Shown in Figure 5.

Shape	Magnetic Field (T)	Current (MA)	Inverse Aspect Ratio	β_{max} Ballooning	β_{max} External Kink
26087	2.87	3.17	0.357	4.3	7.2
Slim	3.0	3.0	0.302	4.9	3.8
Fat	3.0	3.0	0.332	4.3	4.8

The results of this procedure are shown in Fig. 6 and the table. The experimental value of β in the actual discharge was 2.4%, to be compared with the ballooning limit β_{max} = 4.3% and the kink limit β_{max} = 7.2%. This is due to the shape of the current density profile which has only a small gradient near the plasma boundary. However, the new pumped divertor geometries have a much larger influence on the n = 1 external kink mode. The maximum values of β stable to this mode are then 3.8% and 4.8%, respectively. The mode has a global character with a large amplitude across the plasma so that it cannot easily be stabilised by small changes of the current profile at the edge. Consequently, we may expect a different manifestation of the β limit in the divertor experiment. In the case of the 'slim' plasma shape the first ideal mode to become unstable with increasing β is a global n = 1 external kink, leading to a disruption. Clearly, below this limit resistive external modes are also likely to occur.

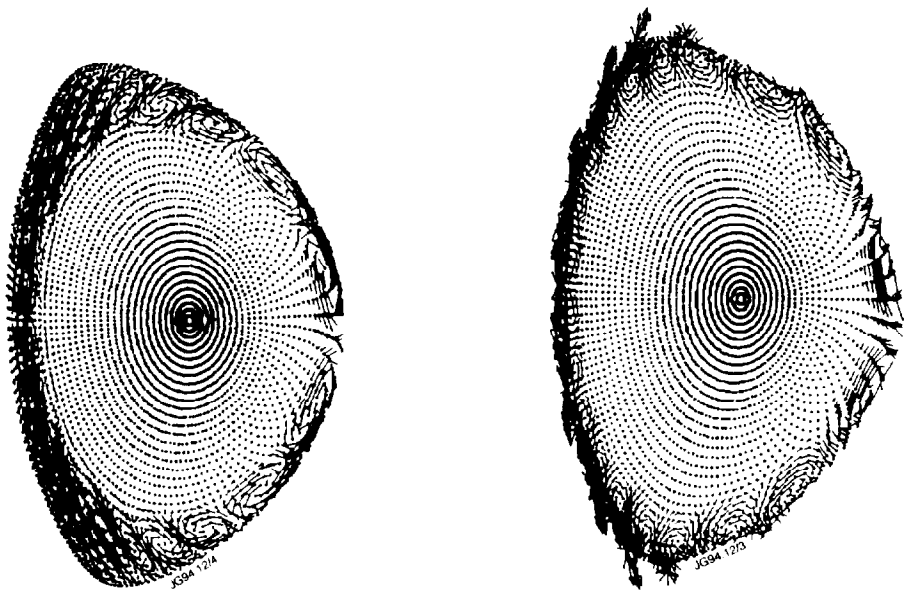

Fig.7. Poloidal Velocities of the n = 4 External Resistive Mode (JET #27793).

- *Influence of the edge pressure gradient, current density, and resistivity* (JET #27793). Returning to external resistive modes, we now include higher values of the toroidal mode number (up to n = 4) and, also, study the influence of the edge pressure gradient since this is more important for these higher mode numbers. In the mentioned discharge ELMs were triggered by the influx of Be impurities presumably leading to a rapid increase of the resistivity. The reconstructed equilibrium did not have large local gradients at the edge. Hence, we again played with the profiles to increase the edge gradients, within experimental uncertainty, up to the

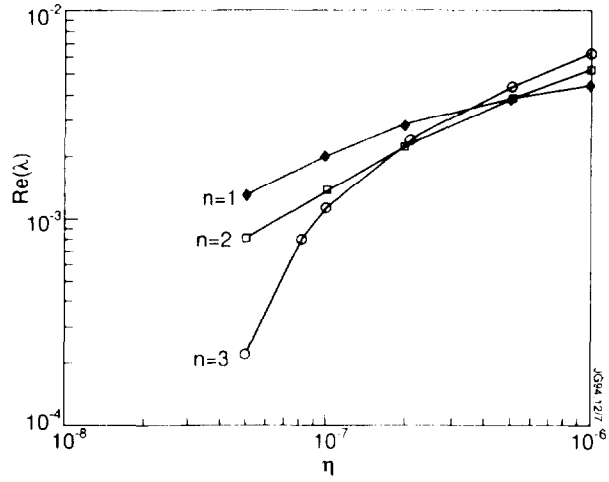

Fig.8. Growth Rates for the n = 1-3 Modes as a Function of the Resistivity.

point where the plasma becomes unstable. First, increasing the pressure gradient, pressure driven modes become unstable. An example is shown in Fig. 7 on the left. Although the calculations were done using a 'free' boundary condition, the n = 4 mode is essentially an internal mode with the largest amplitude at the q = 3 surface and almost no perturbation at the plasma boundary. Also notice that this mode does not show any significant ballooning effect. However, if the current density gradient is also increased (up to the point where the resistive n = 1 current driven mode becomes unstable) the mode structure of the n = 4 mode changes completely, as shown on the right hand side of Fig. 7. In this case the free boundary is essential and the mode has a large amplitude at the plasma boundary.

With decreasing resistivity, the modes are stabilised due to favourable average curvature. This is shown in Fig. 8. The growth rates of the higher n modes decrease faster with increasing n. Hence, the question of which mode number is most unstable depends sensitively on the actual value of the resistivity. From the plot it is clear that for ELMs triggered by an increase of the resistivity by some impurity influx, the lowest n will be the first to become unstable.

4. EXTERNAL EXCITATION OF TAE MODES

4.1 A New Prospect for MHD Spectroscopy

Due to the poloidal coupling of the ideal MHD continuous spectra in toroidal systems [12], gaps appear in which global Alfvén waves (termed TAE modes) may be found. These modes are naturally excited by energetic particles (neutral beam injection, fusion α-particles) and, in turn, these destabilised global Alfvén modes may cause severe losses of α-particles in future ignited plasmas. Hence, a lot of research is devoted to possible damping mechanisms [13].
At JET an experiment is planned to artificially excite these waves by means of an external antenna. To this end, the newly installed saddle coils for disruption control (see Fig. 9) are adapted to permit scanning of the driving frequency in the Alfvén frequency range of 30 - 500 kHz. The frequencies of the TAE modes will show up as resonances of the power absorbed by the plasma, as can be measured by the antenna impedance: an exciting new way of performing MHD spectroscopy!

4.2 Continuous Spectra, Gaps and Damping of Global Alfvén Waves

We recall the construction of the continuous spectra since this is essential for the understanding of the structure of the entire spectrum. By means of an orthogonal projection onto the significant directions $\mathbf{n} \equiv \nabla\Psi / |\nabla\Psi|, \mathbf{b} \equiv \mathbf{B}/B$, $\boldsymbol{\pi} \equiv \mathbf{b} \times \mathbf{n}$, modes localised about a single magnetic surface,

$$\xi(\Psi,\ \theta,\ \varphi) \approx -i\delta(\Psi - \Psi_0)\left[\eta(\theta)\boldsymbol{\pi} + \zeta(\theta)\mathbf{b}\right]e^{in\varphi}, \tag{15}$$

turn out to satisfy a system of two ODE's [12]:

$$\begin{pmatrix} \frac{B}{RB_p} F \frac{R^2B_p^2}{B^2} F \frac{B}{RB_p} + \frac{4\gamma pB^2}{\gamma p + B^2}\kappa_g^2 & -i\frac{2\gamma pB^2}{\gamma p + B^2}\kappa_g F \frac{1}{B} \\ i\frac{1}{B} F \frac{2\gamma pB^2}{\gamma p + B^2}\kappa_g & \frac{1}{B} F \frac{\gamma pB^2}{\gamma p + B^2} F \frac{1}{B} \end{pmatrix} \begin{pmatrix} \eta \\ \zeta \end{pmatrix} = \rho\omega^2 \begin{pmatrix} \eta \\ \zeta \end{pmatrix}, \tag{16}$$

where $F \equiv -i\mathbf{B}\cdot\nabla$ is the parallel gradient operator and $\kappa g \equiv \mathbf{b}\cdot\nabla\mathbf{b}\cdot\boldsymbol{\pi}$ is the geodesic curvature. In a straight cylinder the off-diagonal terms disappear and the Alfvén and slow continua are given by the expressions

$$\omega_A \approx \pm\ F_0 / \sqrt{\rho},\ F_0 \equiv \left(B_\varphi / R\right)\left(n + m / q\right),$$

$$\omega_S \approx \pm \left[\frac{\gamma p}{\gamma p + B^2}\right]^{1/2} F_0 / \sqrt{\rho}. \qquad (17)$$

In toroidal systems, poloidal mode coupling causes 'gaps' to appear between the continuum branches with different poloidal wave numbers m and m', avoiding the crossing of the modes at the rational surfaces where the safety factor q = -(m + m')/2n. The size of these gaps is proportional to the strength of the mode coupling. Moreover, according to Eq. (16), Alfvén and slow continua also become coupled through the combined effect of finite compressibility (γp terms) and geodesic curvature $\left(\kappa_g\right)$.

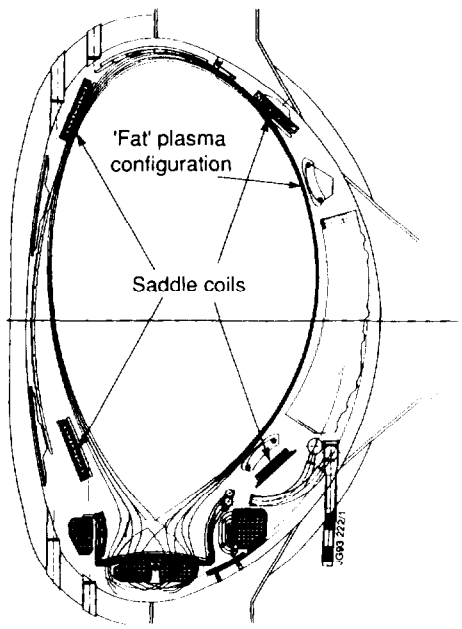

Fig.9. Cross Section of the JET Divertor Geometry Showing the Poloidal Position of the Saddle Coils. There are Four Toroidal Coils at the Top and at the Bottom of the Vessel.

When the poloidal mode coupling is strong enough, global Alfvén modes are found with a frequency in the above mentioned gaps. These 'gap modes' might play an important role in controlled thermonuclear fusion as they can be destabilised by the interaction with fusion born α-particles. An example of the computation of the continuous spectra, gaps and damped Alfvén modes in these

gaps is shown in Fig. 10. The continua (Fig. 10a) were calculated with a helper code [14] derived from CASTOR, corresponding to the Eqs. (17), whereas CASTOR itself was used to compute the global Alfvén modes in the gaps (indicated by the arrows in Fig. 10b). The interaction of these gap modes with the continuum modes causes phase-mixing so that these modes are damped by the same resonant absorption mechanism that produces Alfvén wave heating [15, 17]. The important question now is which of the two phenomena - destabilisation by interaction with α-particles or damping by interaction with continuum modes - is dominant. Preliminary studies have indicated that dampings in the order of 10% may be obtained.

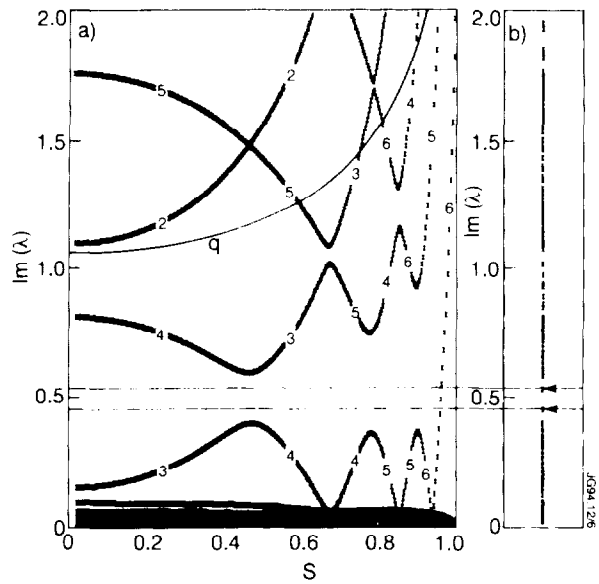

Fig.10. Continuous Spectrum and Gap Modes Obtained from CASTOR for a Model Equilibrium.

4.3 TAE Modes in JET

In Fig. 11 the calculated continua are shown for the JET high performance discharge #26087. On axis the modes are labelled by means of the poloidal mode number m. This labelling completely fails away from axis due to toroidicity, ellipticity, and finite β (β - 2.5% for this discharge). At low frequencies the Alfvén and slow continua are strongly coupled (dotted lines). As a result several 'gaps' appear with possible global modes inside. Rather than computing these with the spectral version of CASTOR (passive boundary perturbation), it is much easier to exploit the active version with the antenna (Sec. 2.2). The response of the plasma due to an n=1 magnetic field perturbation which would induced by the saddle

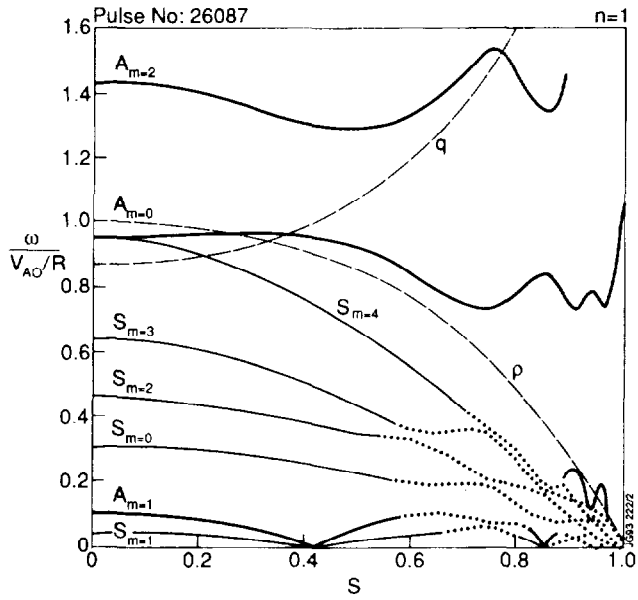

Fig.11. Alfvén and Slow Continua as a Function of the Radial Coordinate $s = \sqrt{\Psi / \Psi_1}$ *for JET Discharge #26087.*

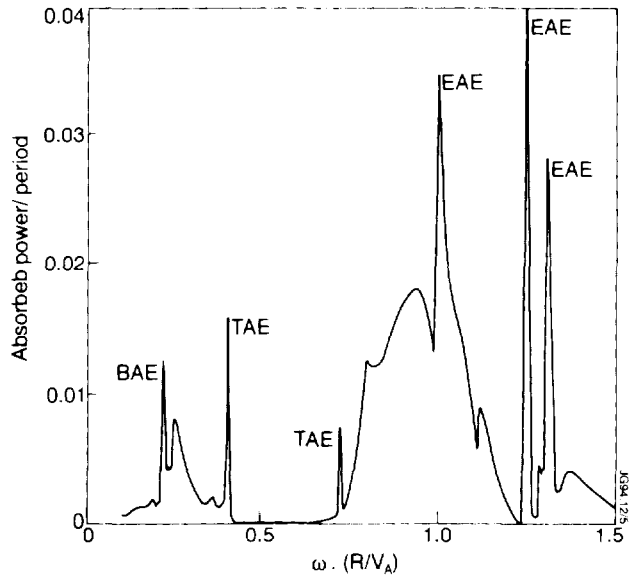

Fig.12. Power Absorbed by the Plasma as a Function of the Normalised Antenna Frequency (n = 1, $\eta = 10^{-7}$, V_A/R - *332 kHz).*

coils is shown in Fig. 12. On top of the broad continuum shoulders several sharp peaks are found labelled with TAE (toroidicity induced:Δm = 1 couplings dominate in the eigenfunctions), EAE (ellipticity induced: Δm = 2 couplings), and BAE (β induced, actually compressibility induced: γp). As may be deduced from the corresponding eigenfunctions, these peaks are indicative of the background plasma equilibrium profiles. If such peaks in the antenna impedance

[18-20] are observed in the future, and, next, correlated with the background profiles, a start will have been made with MHD spectroscopy! From the example of helioseismology, we may then hope to gradually improve the predictive power of MHD calculations.

5. CONCLUSIONS

- External low to intermediate n resistive free-boundary MHD modes are likely candidates to explain ELMs in JET: they occur well below the ideal ballooning limit, they involve large perturbations of the boundary they involve small current profile changes at the edge, and they exhibit a sharp dependence on the edge resistivity.

- Excitation of MHD modes by means of an external antenna may turn out to be a great diagnostic instrument: MHD spectroscopy is about to be born.

- A promising aspect of the external excitation of TAE modes is that the experiment has a knob to control the level of excitation, so that in principle a continuous transition from the linear to the non-linear regime can be made (if there is sufficient power). This is a definite advantage as compared to the situation in helioseismology. On the other hand, since the presently considered antenna power is still small, we will have a controlled situation where the modes are likely to remain in the linear regime so that the given theoretical description should be valid.

ACKNOWLEDGEMENTS

This work was performed as part of the research programme of the association agreement of Euratom and the 'Stichting voor Fundamenteel Onderzoek der Materie' (FOM) with financial support from the 'Nederlandse Organisatie voor Wetenschappelijk Onderzoek' (NWO) and Euratom. It was supported by the grants JT2/10327 and JT2/12405 of the JET Joint Undertaking.

REFERENCES

[1] J.P. Goedbloed, 1991, 'MHD Waves in Thermonuclear and Solar Plasmas', in Trends in Physics, ed(s). Kaczér, J., EPS. Prague, III, 827.

[2] J.P. Goedlboed, G.T.A. Huysmans, S. Poedts, G. Halberstadt, W. Kerner, E. Schwarz, 1992, 'Computation of Resistive MHD Modes in Thermonuclear and Astrophysical Plasmas' in Proc. IAEA Technical Committee Meeting on Advances in Simulation and Modeling of Thermonuclear Plasmas, Montréal, ed(s). V. Demchenko, M. Shoucri, IAEA. Vienna 316.

[3] W. Unno, Y. Osaki, H. Ando, H. Saio, H. Shibahashi. 1989, 'Nonradial Oscillations of Stars', University of Tokyo Press: Tokya, 321.

[4] J. Christensen-Dalsgaard, 1989, 'Stellar Oscillations', Astronomisk institut, Aarhus Universitet, 52.

[5] I.B. Bernstein, E.A. Frieman, M.D. Kruskal, R.M. Kulsrud, 1973, 'An Energy Principle For Hydromagnetic Stability Problems', Proc. Roy. Soc. **A244**, 17.

[6] W. Kerner, 1989, 'Large-scale Complex Eigenvalue Problems', Journal of Computational Physics **85**, 1.

[7] G.T.A. Huysmans, J.P. Goedbloed, W. Kerner 1991, 'Isoparametric Bicubic Hermite Elements for Solution of the Grad-Shafranov Equation', in Computational Physics, ed(s). A. Tenner World Scientific. Singapore, 371.

[8] G.T.A. Huysmans, J.P. Goedbloed, W. Kerner 1993, 'Free Boundary Resistive Modes in Tokamaks', Phys. Fluids **B5**, 1545.

[9] R.J. Groebner 1993, 'An emerging Understanding of H-mode Discharges in Tokamaks', Phys. Fluids **B5**, 2343.

[10] N. Hawkes, 1993, 'Electric Field Measurements During the H-Mode in JET', in Proc 20th Eur. Conf. on Controlled Fusion and Plasma Physics, ed(s). J.A. Costa Cabral, M.E. Manso, F.M. Serra, F.C. Schüller, EPS Lisbon, I, 3.

[11] G.T.A. Huysmans, H.J. de Blank, W. Kerner, J.P. Goedbloed, M.F.F. Nave. 1992, 'MHD Stability Models of Edge Localised Modes in JET Discharges', in Proc. 19th Eur. Conf. on Controlled Fusion and Plasma Physics, ed(s). W. Freysinger, K. Lackner., R. Schrittwieser, W. Lindinger. EPS Innsbruck, I, 247.

[12] J.P. Goedbloed, 1975, 'Spectrum of Ideal Magnetohydrodynamics of Axisymmetric Toroidal Systems', Phys. Fluids **18**, 1258.

[13] A.D. Turnbull, E.J. Strait, W.W. Heidbrink, M.S. Chu, H.H. Duong, J.M. Greene, L.L. Lao, T.S. Taylor, S.J. Thompson. 1993 'Global Alfvén Modes: Theory and Experiment', Phys. Fluids **B5**, 2546.

[14] S. Poedts and E. Schwarz 1992, 'Computation of the Ideal MHD Continuous Spectrum in Axisymmetric Plasmas', J. Comp. Physics **105**, 165.

[15] S. Poedts, W. Kerner, M. Goossens, 1989, Alfvén-wave Heating in Resistive MHD', J. Plasma Physics **42**, 27.

[16] W. Kerner, S. Poedts, J.P. Goedbloed, G.T.A. Huysmans, B. Keegan, E. Schwarz 1991, 'Computing the Damping and Destabilization of Global Alfvén-waves in Tokamaks', in Proc. 18th Eur. Conf. on Controlled Fusion and Plamsa Physics. ed(s). P. Bachmann, D.C. Robninson, EPS Berlin, IV, 89.

[17] S. Poedts, W. Kerner, J.P. Goedbloed, B. Keegan, G.T.A. Huysmans and E. Schwarz, 1992, 'Damping of Global Alfvén-waves in Tokamaks due to Resonant Absorption', Plasma and Physics and Controlled Fusion **34**, 1397.

[18] G.T.A. Huysmans, H. Holties, W. Kerner, J.P. Goedbloed, D. Borba, F. Porcelli, 1993, 'MHD Spectroscopy: Modelling the Excitation of TAE Modes by an External Antenna', in Proc. 20th Eur. Conf. Controlled Fusion and Plasma and Plasma Physics, ed(s). J.A. Cabral Costa, M.E. Manso, F.M. Serra, F.C. Schüller, EPS Lisbon I, 187.

[19] W. Kerner, D. Borba, G.T.A. Huysmans, F. Porcelli, S. Poedts, J.P. Goedbloed, R. Betti, 1993. 'Stability of Global Alfvén Waves (TAEs, EAE) in JET Tritium Discharges', in Proc. 20th Eur. Conf. on Controlled Fusion and Plasma Physics, ed(s). J.A. Cabral Costa, M.E. Manso, F.M. Serra, F.C. Schüller, EPS Lisbon, I, 183.

[20] L. Villard, J. Vaclavik, S. Brunner, H. Lütjens, A. Bondeson, 1993, 'Alfvén Gap Modes in Elongated Plasmas', in Proc. 20th Eur. Conf. on Controlled Fusion and Plasma Physics, ed(s). J.A. Costa Cabral, M.E. Manso, F.M. Serra, F.C. Schüller, EPS, Lisbon, IV, 1347.